NANO EXPRESS

Photoluminescence Study of Low Thermal Budget III–V Nanostructures on Silicon by Droplet Epitaxy

S. Bietti · C. Somaschini · E. Sarti ·
N. Koguchi · S. Sanguinetti · G. Isella ·
D. Chrastina · A. Fedorov

Abstract We present of a detailed photoluminescence characterization of high efficiency GaAs/AlGaAs quantum nanostructures grown on silicon substrates. The whole process of formation of the GaAs/AlGaAs active layer was realized via droplet epitaxy and migration enhanced epitaxy maintaining the growth temperature ≤350°C, thus resulting in a low thermal budget procedure compatible with back-end integration of the fabricated materials on integrated circuits.

The possibility to integrate opto-electronic and photonic devices, based on III–V semiconductors, directly on Si-based integrated circuits (IC) is one of the major research issues of today microelectronics industry [1–6]. Of particular technological interest is the possibility of carrying out the III–V device fabrication as a back-end process, that is, after the IC has been already realized. In this case, strict constraints on thermal budget for growth and processing of the epilayer are imposed by the compatibility with the underlying IC.

Integration of III–V materials on silicon is far from being optimized. Several important challenges have to be overcame in order to obtain high-quality III–V material on Si: the large lattice mismatch between GaAs and Si (about 4.1%), which introduces a large number of misfit dislocations as soon as GaAs epilayer exceeds a critical value, the formation of Anti-Phase Domains (APDs) and the strict thermal budget required during the growth of a GaAs epilayer to maintain the compatibility with the underlying IC. To partially release these issues, a Ge virtual substrate (GeVS) deposited on Si miscut wafers is commonly used [7]. Thermal budget constraints, however, still constitute a major problem when back-end integration is pursued.

Here, we present a detailed photoluminescence characterization of high-efficiency GaAs/AlGaAs quantum nanostructure directly realized on Si by a droplet epitaxy (DE) [8, 9]. The nanostructures, made by a complex ring–disk coupled nanostructure, show a bright emission, still visible at room temperature. Of fundamental importance, DE is *intrinsically* a low thermal budget growth being performed at 200–350°C. This makes DE perfectly suited for the realization of growth procedures compatible with back-end integration of III–V nanostructures on ICs.

The DE, a molecular beam epitaxy (MBE)—based growth method for the fabrication of three–dimensional nanostructures [10, 11], has demonstrated an unmatched ability to produce nanometer size islands of III–V semiconductors, in both lattice-matched and lattice-mismatched materials [12, 13], with complex, designable,and geometries [14, 15]. Unlike the standard MBE growth, where the constituent elements are simultaneously supplied onto the substrate surface, the DE is based on the sequential supply of III-column and V-column element. In the case of DE growth, first lots of nanometric metallic droplets with homogeneous size are formed by group III irradiation in absence of As and then, in order to obtain the crystallization of the Ga droplets, an As flux is supplied. By choosing

S. Bietti · C. Somaschini · E. Sarti · N. Koguchi ·
S. Sanguinetti (✉)
L-NESS and Dipartimento di Scienza dei Materiali,
Via Cozzi 53, 20125 Milano, Italy
e-mail: stefano.sanguinetti@mater.unimib.it

G. Isella · D. Chrastina · A. Fedorov
CNISM, L-NESS and Dipartimento di Fisica del Politecnico di
Milano, Via Anzani 42, 22100 Como, Italy

suitable growth conditions, the As flux transforms the metallic droplets into nanometer size islands.

In this work, Si(001) substrates, 6° misoriented towards [110], were used to allow growth of GaAs layers free of APDs [16]. A 2 μm Ge fully relaxed layer, acting as GeVS, was deposited at 500°C by low-energy plasma-enhanced chemical vapor deposition (LEPECVD) [17]. The threading dislocation density was reduced to $2 \times 10^7 \mathrm{cm}^{-2}$ by six in situ UHV thermal annealing cycles between 600 and 780°C [18, 19]. The GeVS was then transferred to a Gen II MBE system. A buffer layer of 1 μm GaAs was first grown on top of the GeVS at 580°C. Using reflection high-energy electron diffraction (RHEED), we observed a clear (2 × 4) surface reconstruction, confirming APD-free growth. On top of the buffer, the nanostructured active layer was realized. At first, the temperature was decreased to 350°C, and an 80 nm $Al_{0.30}Ga_{0.70}As$ barrier was grown by migration-enhanced epitaxy (MEE) [20] to assure high crystal quality also at such a low growth temperature. DE was performed at the same temperature. After the removal of As from the growth chamber, 10 ml of Ga was deposited. The formation of tiny droplets Ga on the AlGaAs surface was checked by atomic force microscopy (AFM) measurements. Then, an As flux with a beam equivalent pressure (BEP) of 8×10^{-6} Torr was directed onto the sample for 20 min in order to completely crystallize the Ga droplet into a quantum nanostructure. The RHEED pattern confirmed the formation of nanostructures by the appearance of transmission spots. The atomic force microscope (AFM) image of the surface at this stage of the growth is shown in Fig. 1. The produced nanostructures are characterized by a regular, nanometers high, flat disk with a diameter of hundreds of nanometers and a hole at the center of ≈ 80 nm. The rim of the inner hole is protruded over the disk surface by some nanometers. We call these structured coupled ring disks (CRD). The measured CRD density is $\rho = 6 \times 10^8 \mathrm{cm}^{-2}$. The low temperature $(T = 14$ K) photoluminescence of the grown sample was finally capped with 80 nm of $Al_{0.30}Ga_{0.70}As$ and 10 nm of GaAs at the same temperature and subjected to rapid thermal annealing at 600°C for 4 min. The PL spectra were measured at 14 K using a closed-cycle cold-finger cryostat at room temperature (RT). PL was excited with a Nd:YAG laser $(\lambda_{exc} = 532$ nm) with an excitation power density $P_{exc} = 6$ W/cm^2. The spectra were measured by a grating monochromator operating with a Peltier-cooled CCD detector.

These structures constitute the good example of nanostructures with coupled localized–extended states with cylindrical symmetry (the protrusion at the inner ring edge acts, in fact, as three-dimensional electronic carrier confinement potential, thus being like a ring laid down on top of quantum disk), thus offering additional degrees of

Fig. 1 AFM scan (1 μm × 1 μm) of GaAs CRDs grown on a GeTVS

freedom for the control of effective coupling between excitons trapped in quantum nanostructures [21]. The PL spectra at $T = 14$ K of the sample is reported in Fig. 2. An intense and broad band is clearly visible in at 1.55 eV, with a full width at half maximum of ≈ 30 meV, well above the GaAs-related impurity lines. The band shows a shoulder at 1.60 eV. In order to attribute these lines, we calculated the theoretical emission energy of CRDs, obtained in the effective mass approximation [22, 23] using as confinement potential of the nanostructure the actual shape of a randomly chosen CRD measured by AFM. The theoretically calculated CRD ground electronic and hole states appear to be confined in the ring structure, which is formed at the edge of the inner CRD hole. The calculated emission energy well compares with the observed PL peak value $(E^{th}_{GS} = 1.56$ eV). The low confinement energy $(\approx 30$ meV) is due to the relatively large, but still capable of quantum confinement, thickness. The CRD excited state is, on the other side, a quantum well-like state extended along the disk $(E^{th}_{EX} = 1.59$ eV). For the calculations, we used the materials parameters reported in Ref. [24] for GaAs and $Al_{0.3}Ga_{0.7}As$. The interdiffusion at the CRD interface, which takes place in DE material during annealing [25, 26], was taken into account [23].

The PL spectra evolution with the temperature is shown in Fig. 3a. The CRD emission red shifts, as expected, with the increasing temperature. As the temperature increases, the emission from the excited state gains in relative strength respect to the ground state. The CRD band is still clearly visible at RT and centered at 1.515 eV where is dominated by the excited state emission. The ratio between the integrated intensity of the two bands, reported in Fig. 3b, shows an activation energy of ≈ 45 meV, which corresponds to the energy difference between ground and excited state emission. The CRD PL integrated intensity
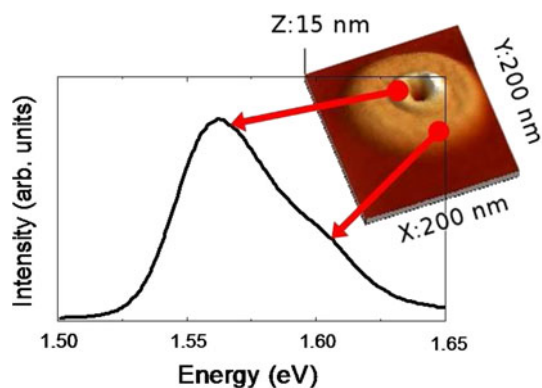
Fig. 2 PL spectrum of the CRD sample at low temperature ($T = 14$ K). *Upper right corner* AFM image of a single CRD. The emission at 1.55 eV is attributed to carriers confined in the ring protrusion of the CRD, while the shoulder at 160 eV to states belonging to the disk

Fig. 4 Integrated Intensity dependence on temperature of the CRD PL

(see Fig. 4a) is reduced by a factor ≈ 400 respect to the low temperature case. The PL integrated intensity Arrhenius plot (Fig. 4) shows a clear temperature activated quenching, with a measured activation energy $E_{QUE} \approx 100$ meV.

Let us discuss the phenomenology presented. The quenching process while showing a low quenching energy ($E_{QUE} \approx 100$ meV) is relatively mild (a factor 400 reduction between 14 K and RT). In addition, E_{QUE} is much smaller than any energy barrier in the CRD system. It must be therefore attributed to a non-radiative recombination defect with small cross section, directly accessible from CRD, or to the quenching active during the carrier diffusion and capture process [27]. The latter has been demonstrated to be present in DE materials [26]. As far as the change in spectral weight as the temperature increases is concerned, we found a presence of an activation energy, which corresponds to the ground to excited state energy
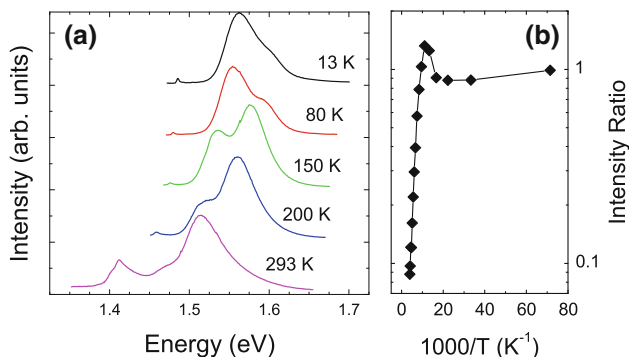
difference. Is it then possible to attribute the relative increase of excited state emission to a change in equilibrium population of ground and excited states. As the temperature increase, the population ratio of the two states evolves according to the Fermi law. The predominance of disk emission respect to the ring one at RT should comes from the strongly different density of states (much higher in the disk case) attributable to the different dimensionality of the two CRD sub-systems (0D for the ring and 2D for disk).

In order to assess the quality of the realized structures, we determined the ratio η between the number of photo-generated carriers in the GaAs/AlGaAs active layer and the number of photons emitted by the CRDs. The sample shows $\eta \approx 3 \times 10^{-3}$ at $T = 14$ K and $P_{exc} = 6$ W/cm^2. This values well compare with $\eta \approx 1 \times 10^{-2}$ relative to a standard DE quantum dot sample with similar ($\rho = 1.2 \times 10^9$ cm^{-2}) nanostructure density (sample D680 of Ref. [28]). No dependence of η on P_{exc} was found at low temperatures. η naturally drops to $\eta \approx 8 \times 10^{-6}$ at RT due to temperature activated non–radiative recombination channels. A marked superlinearity in the quantum yield ($\eta \propto P_{exc}^\alpha$) is observed at RT with α close to two. Such behavior has been already reported in quantum dot structures and attributed to the saturation of non–radiative recombination channels in the barrier active during carrier diffusion processes [27].

In conclusion, we presented the PL behavior of high-efficiency GaAs/AlGaAs quantum nanostructures realized on silicon using a low thermal budget procedure suitable for IC integration.

Fig. 3 a CRD PL spectra in the 14–300 K temperature range. The spectra are normalized ad shifted for clarity. **b** Arrhenius plot of the ground and excited states integrated intensity ratio
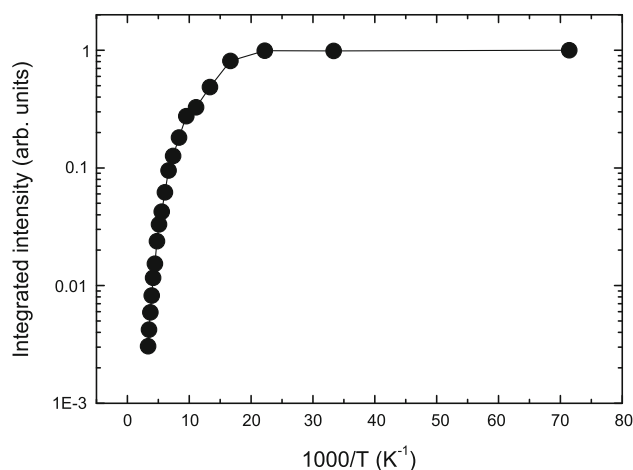
References

1. E.A. Fitzgerald, Y.-H. Xie, D. Monroe, P.J. Silverman, J.M. Kuo, A.R. Kortan, F.A. Thiel, B.E. Weir, J. Vac. Sci. Technol. B **10**, 1807 (1992)
2. J. De Boeck, G. Borghs, J. Cryst. Growth **127**, 85 (1993)
3. Y. Chriqui, G. Saint-Girons, S. Bouchoule, J.-M. Moisons, G. Isella, H. von Kaenel, I. Sagnes, Electron. Lett. **39**, 1658 (2003)
4. Y. Chriqui, L. Largeau, G. Patriarche, G. Saint-Girons, S. Bouchoule, I. Sagnes, D. Bensahel, Y. Campidelli, O. Kermarrec, J. Cryst. Growth **265**, 53 (2004)
5. Y. Chriqui, G. Saint-Girons, G. Isella, H. von Kaenel, S. Bouchoule, I. Sagnes, Opt. Mater. **27**, 846 (2005)
6. P. Chen, Y. Jing, S.S. Lau, D. Xu, L. Mawst, T.L. Alford, C. Paulson, T.F. Kuech, Appl. Phys. Lett. **92**, 092107 (2008)
7. S.M. Ting, E.A. Fitzgerald, I. Introduction, J. Appl. Phys. **87** (2000).
8. N. Koguchi, S. Takahashi, T. Chikow, J. Cryst. Growth **111**, 688 (1991)
9. N. Koguchi, K. Ishige, Jpn. J. Appl. Phys. **32**, 2052 (1993)
10. N. Koguchi, S. Takahashi, T. Chikyow, J. Cryst. Growth **111**, 688 (1991)
11. N. Koguchi, K. Ishige, Jpn. J. Appl. Phys. **32**, 2052 (1993)
12. K. Watanabe, N. Koguchi, Y. Gotoh, Jpn. J. Appl. Phys. **39**, L79 (2000)
13. T. Mano, K. Watanabe, S. Tsukamoto, N. Koguchi, H. Fujioka, M. Oshima, C. Lee, J. Leem, H.J. Lee, S.K. Noh, Appl. Phys. Lett. **76**, 3543 (2000)
14. T. Mano, T. Kuroda, S. Sanguinetti, T. Ochiai, T. Tateno, J. Kim, T. Noda, M. Kawabe, K. Sakoda, G. Kido et al., Nano Lett. **5**, 425 (2005)
15. C. Somaschini, S. Bietti, N. Koguchi, S. Sanguinetti, Nano Lett. **9**, 3419 (2009)
16. S.M. Ting, E.A. Fitzgerald, J. Appl. Phys. **87**, 2618 (2000)
17. G. Isella, D. Chrastina, B. Rössner, T. Hackbarth, H.-J. Herzog, U. König, H. von Känel, Solid State Electron **48**, 1317 (2004)
18. G. Isella, J. Osmond, M. Kummer, R. Kaufmann, H. von Känel, Semicond. Sci. Technol. **22**, S26 (2007)
19. J. Osmond, G. Isella, D. Chrastina, R. Kaufmann, M. Acciarri, H. von Känel, Appl. Phys. Lett. **94**, 201106 (2009)
20. Y. Horikoshi, M. Kawashima, H. Yamaguchi, Jpn. J. Appl. Phys. **27**, 169 (1988)
21. L.G.G.V. Dias da Silva, J.M. Villas-Bôas, S.E. Ulloa, Phys. Rev. B **76**, 155306 (2007)
22. J.Y. Marzin, G. Bastard, Solid State Commun. **92**, 437 (1994)
23. S. Sanguinetti, K. Watanabe, T. Kuroda, F. Minami, Y. Gotoh, N. Koguchi, J. Cryst. Growth **242**, 321 (2002)
24. T. Kuroda, T. Mano, T. Ochiai, S. Sanguinetti, K. Sakoda, G. Kido, N. Koguchi, Phys. Rev. B **72**, 205301 (2005)
25. V. Mantovani, S. Sanguinetti, M. Guzzi, E. Grilli, M. Gurioli K. Watanabe, N. Koguchi, Physica E **23**, 377 (2004)
26. S. Sanguinetti, T. Mano, A Gerosa, C. Somaschini, S. Bietti, N. Koguchi, E. Grilli, M. Guzzi, M. Gurioli, M. Abbarchi, J. Appl. Phys. **104**, 113519 (2008)
27. S. Sanguinetti, D. Colombo, M. Guzzi, E. Grilli, M. Gurioli, L. Seravalli, P. Frigeri, S. Franchi, Phys. Rev. B **74**, 205302 (2006)
28. V. Mantovani, S. Sanguinetti, M. Guzzi, E. Grilli, M. Gurioli, K. Watanabe, N. Koguchi, J. Appl. Phys. **96**, 4416 (2004)